AIAA 96-3204

Design, Fabrication and Testing of 30-cm Dia. Dished Carbon-Carbon Ion Engine Grids

Juergen Mueller, John R. Brophy and D. Kyle Brown

Jet Propulsion Laboratory
California Institute of Technology
Pasadena, CA 91109

32nd AIAA/ASME/SAE/ASEE
Joint Propulsion Conference and Exhibit
July 1-3, 1996 / Lake Buena Vista, FL

AIAA 963204

Design, Fabrication and Testing of 30-cm dia. Dished Carbon-Carbon Ion Engine Grids

Juergen Mueller", John R. Brophy**, and D. Kyle Brown***

Jet Propulsion Laboratory
California in.vtit14tr of Technology
Pasadena, CA 91109

Two *sets of* 30-cm dia. dished carbon-carbon Ion **engine** grid sets were fabricated, assembled and tested. **The** carbon-carbon grid blanks were **fabricated** from unidirectional **prepreg** tape, having a very high fiber volume fraction of **57%** and **resulting** in the strongest quasi-isotropic **carbon - carbon material** known to the authors. **The flexural modulus** of **the** panel material was measured at 27S **MPa,** corresponding **to 80%** Of **the value** for molybdenum. Grid hoie apertures **were** machined **by laser-cutting.** Inspection of the grid after fabrication revealed very tight hole tolerances, however, **radii** of curvature of the screen, accelerator and decelerator grids were **larger** than specified. **The** data indicate a correlation between radius of curvature and open-area-fraction of the grid, **possibly** caused **by** the laser-fabrication process. **To min Imize the** impact of the larger screen **grid** radius of curvature relative to the accelerator grid, **the grids** were mounted dished inward. **Perveance** and **electron backstreaming** limits were measured. At 1.7 A screen current the **perveance limit** was found to **be** 1.4 **kV** and at 1.0 A screen current it was **1.0** kV. **The electron backstreaming** limit was -130 **V** at **1.7** A rrod .9S V at **1.0A.**

Introduction

Carbon-carbon grid technology for usc in ion engine acc.clc.rater systems has been under investigation by various researchers[1-10] for several years now, Initial results of these investigations have been very encouraging due to material properties which make carbon-carbon attractive for usc as a grid material. Carbon-carbon composites consist of a graphitic fiber in a carbonaceous matrix, consisting in turn partly of a graphitic and a glassy carbon phase.. Due to this composition of materials, carbon-carbon exhibits the low sputter yields of graphite, yet at considerably higher structural strength than graphite alone. Blandino et al." was able to show that carbon-carbon wear rates due to xenon ion sputter erosion arc very similar to those found for graphite and consequentl y obtained wear rates of carbon-carbon vs. molybdenum of 1:7.3 and 1:7.7 at xenon ion energies of 500 eV and 750 cV, respectively.

This reduced wear rate translates directly into longer ion accelerator grid lifetimes which will increase overall ion engine life. Typical ion engine w-vice requirements are many thousand hours for missions to the outer planets, the. Kuiper-Belt, the main belt asteroids, and comets. The NASA Solar Electric Propulsion Technology Applications Readiness (NSTAR) program, which seeks to validate ion engine technology for the.sc. types of missions, has a service life requirement of 8,000 hours, corresponding to a xenon throughput of 83 kg. Often mission scenarios for outer planet and small body missions involve the usc of 1 ion thruster operating sequentially to achieve the required total impulse. The use of ion engines equipped with carbon-carbon grid technology may eliminate grid erosion as the life-lirniting engine phenomena. Longer engine life will enable the use of fewer engines and reduce the propulsion system dry mass, the initial spacecraft wet mass and overall mission cost.

Previous investigations of carbon-carbon grid technology have focused on small (1 O - 15 cm dia.) grids to demonstrate the feasibility of Ibis technology, and were focused primarily on grid fabrication techniques, measurement of material properties such as coefficient of thermal expansion (CTE) and sputter yield, and grid performance parameters (perveance and electron backstreaming). Most recently, two 700-hr ion engine endurance tests with 15-cm grid sets were completed at J PI.[1], showing no detectable evidence of carbon-carbon grid erosion over the duration of the tests. In addition, a unique. grid configuration with non-circular grid hole apertures has been investigated[2].

"Member of Technical Staff, Advanced Propulsion and Technology Group, Member AIAA
**Group Supervisor, Advanced Propulsion and Technology Group, Member AlAA
***Member of Technical Staff, Space. Materials Science Section, Member AlAA

This paper focuses on the development of 30-cm carbon-carbon grid optics retrofittable to the NSTAR ion engine. The. goal of this activity is to investigate the feasibility of fabrication, assembly and operation of large diameter carbon-carbon grids as a follow-m to the current NSTAR technology. Unique design issue.s to the fabrication, assembly and test of large diameter carbon-carbon grids were to be identified and lessons-learned from this activity will be applied to future designs,

Grid Set Design, Fabrication and Inspection

Grid Panel Fabrication

The carbon-carbon panels for the 30-cm dia. grids were fabricated in part at JPL, BF Goodrich Aerospace, and Accu-Tech Laser Processing, Inc. Grid design, lay-up and curing of the panels were performed at JPL. Chemical vapor infiltration (CVI), carbonization and graphitization stages of the grid fabrication were performed at BF Goodrich Aerospace and machining of the grid apertures, mounting holes and final machining of the. grids were executed at Accu-Tech Laser Processing, using a laser-cutting technique.

The first of the fabrication phases consisted of laying up of the prepreg material in the desired orientation. 1 lere, the lay-up was of the $[0^o/+60^o/-60^o]_s$ type and was performed at JPL using commercial unidirectional prepreg material. Each grid pane.1 consists of a total of six plies, with fibers aligned along -60°, + 60°, 0°,0°, +60° and -60° directions in the. six different plies, respectively. The. lay-up is symmetrical with respect to the centerplane to prevent warpage due. to the highly directional thermal characteristics of the. plies[1,3]. Commercial prepreg tape from YI.A Inc., consisting of DuPont E55 fiber made from pitch based carbon and phenolic resin (Borden SC1008 phenolic) was used for the panel lay-up. A total of six 30-cm grid panels were fabricated, providing enough material for the fabrication of 3 two-grid sets or 2 three-grid sets.

Fabrication of the grid panels is discussed in detail in Ref. 1. Table 1 shows some of the. material properties of the carbon-carbon when compared with carbon-carbon panels of a previous production run for the. fabrication of 15-cm dia. grid panels'. Material properties of the new grid material were obtained by using flat panel material samples from a fabrication run for 1 S-cm dia. grid panels (described in detail in Ref. 1), since the. dished carbon-carbon pane.ls were too expensive to be sacrificed for destructive material testing. However, the. dished carbon-carbon material is identical to the flat carbon-carbon panels of Ref. 1 since it was fabricated from the same prepreg material, featured the same [0°/+60°/-60°], lay-up and underwent the same fabrication procedure.

The high fiber volume and corresponding low carbonized resin content in the. new $[0^o/+60^o/-60^o]_s$ panels, as indicated in I'able 1, is significant in that it resulted in the strongest quasi -isotropic carbon-carbon material known to the authors. The marked increase in the flexural modulus over the previous generation of pane.ls is of particular importance for the intended usc of these panels as ion engine grids. The flexural modulus is a critical grid structural property since it determines how far the grid may bend due. to electrostatic or Vibrational (launch) loads. The value. for the flexural modulus in the 0^o direction of the carbon-carbon panels now reaches about 80% of the. value for molybdenum. However, this increase in flexural modulus in the 0^o direction comes at a price. Due to the higher fiber volume of these panels, lcss cross-linkage is provided by the reduced matrix content and the flexural modulus in the 90^o direction is thus reduced over the val uc found for the previous generation of panels, Thicknesses for the dished panels were. measured at 0.46 mm for all types, i.e. screen accelerator and decelerator grids. Screen grid panels, which have a somewhat smaller diameter, weigh around 95 grams whereas acc.clc.rater and decelerator panels weigh around 108 grams and 105 grams, respectively.

The dished grid blanks were then shipped to Accu-Tech Laser Processing for laser-machining using a 500" W slow flow coaxial CO_2 laser by Photon SourCCs at a 150 W power setting. Spot size of the. laser was 0.005 inch (O. 13 mm). Compressed air was used as a cutting gas to remove debris from the drill site'. No reactive gases were used to aide in the cutting. The grid hole.s were machined by orbiting the narrowly focused laser beam along a path that was to become the hole edge. Earlier tests conducted by the authors with other vendors, using the laser as a drill rather than a cutting lead to disappointing results[4]. However, using the cutting technique mentioned above resulted in exceptional hole quality and outstanding accuracy and repeatability in hole diameter. This laser-cutting technique is very similar to the. onc explored previously by Meserole and Hedges[7-9].

The laser machining included the cutting of the grid holes (about 15,500 pcr grid), as well as the grid mounting holes and finish cutting the grid diameters. Screen, accelerator and decelerator grid dimensions were

Table 1: Material Properties of Carbon-Carbon Panels

Property	Previous Fabrication $[0^0/+60^0/-60^0]_S$	Current Fabrication $[0^0/+60^0/-60^0]_S$
Density (g/cm^3)	1.77	1.83
Thickness (mm)	0.5(1)/0.95(2)	0.46
Fiber by Weight	50.2%	69%
Resin by Weight	17.6%	3-4%
CVI by Weight	32.2%	26-28%
Fiber Volume	40.1%	57%
Resin Volume	16.4%	3%
CVI Volume	30.0%	2-/%
Void Volume	13.6%	13%
Tensile Strength (MPa)	308	486(3)
Tensile Modulus (GPa)	179	]45(3)
Flexural Strength (MPa)	240(1) / 280(2)	205(3) / 117(4)
Flexural Modulus (GPa)	210(1) / 161(2)	275(3) / 61(4)

(1)Screen Grid
(2)Accelerator/Decelerator Grid
(3)0° Direction
(4)90° Direction

dictated by the requirement to make this grid set retrofittable to the NSTAR engine. Photographs of the three of the six grids arc shown in Figs 1, 2, and 3, respectively. Two tags arc visible on all three grids shown in these figures. The arrow indicates the, clocking hole with respect to which contour and grid hole measurements were taken. The second tag is a grid identification mark.

Grid dimensions for the three grid types arc listed in I'able 2. The screen grid has an outer diameter of 35.06 cm with tbc hole pattern area extending over a diameter of 28.58 cm (active beam area). The dished area of the screen grid is 33.17 cm in diameter, leaving a flat annulus around the dish which serves as a mounting flange for the grid. The design value for the radius of curvature for the grid was 203.2 cm, however, as will be discussed below, the final dish depth was found to be smaller than the design value.. Twelve. mounting holes were laser-cut equidistantly on a bolt circle of 34.11 cm into the flat flange outside. the dished region. The grid hole sizes were measured to be 1.89 mm dia. with very little deviation (+ 0.002S mm/-0.009 mm). Grid hole spacing is 2.21 mm center-to-center 011 all three grids. The open area fraction of the grid can then be calculated according to

$$OAF = \frac{\pi d^2}{6c^2 \tan 30^\circ} \qquad (1)$$

where *d is the.* hole. diameter and *c* the center-to-center hole. spacing. For the values given above, the. screen grid open area fraction is 66%.

The accelerator grid is of the SIIAG-type (small hole accelerator grid) and larger in diameter (38.06 cm) than the screen grid. Twelve mounting holes arc located on a 36.73 cm dia. bolt circle. Clearing holes for screws mounting the decelerator grid arc located on the. same bolt circle. clocked 15° and clearing holes for the heads of screws used to mount the. screen grid beneath the

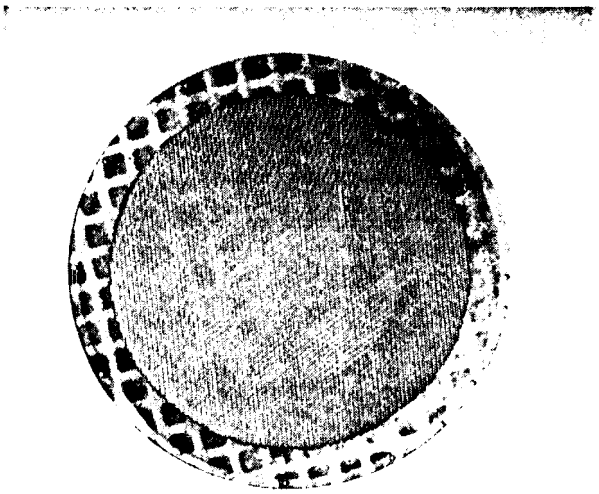

Fig. 1: Screen Grid

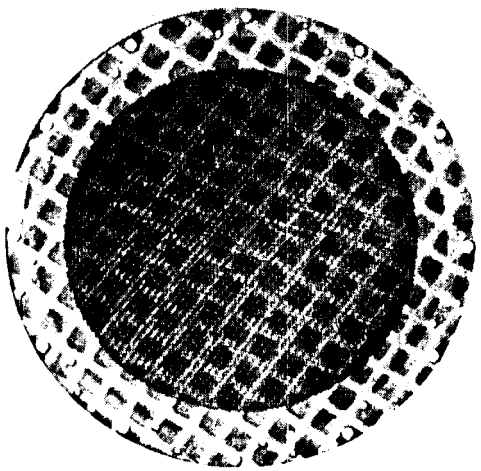

Fig. 2: Accelerator Grid

accelerator grid are located on a 34.11 cm bolt circle. Clearing holes for the screw heads prevent contact between grids. The accelerator grid dished area is the same as the screen grid. Hole diameters were measured to be 1.13 m m and again very little deviation from the mean hole diameter can be noted (± 0.02 mm). From the average hole diameter and the grid hole spacing of 2.21 mm, the open area fraction of the accelerator grid is calculated to 23.5 %.

The decelerator grid has the same OD as the accelerator grid and the same dished area as the screen and

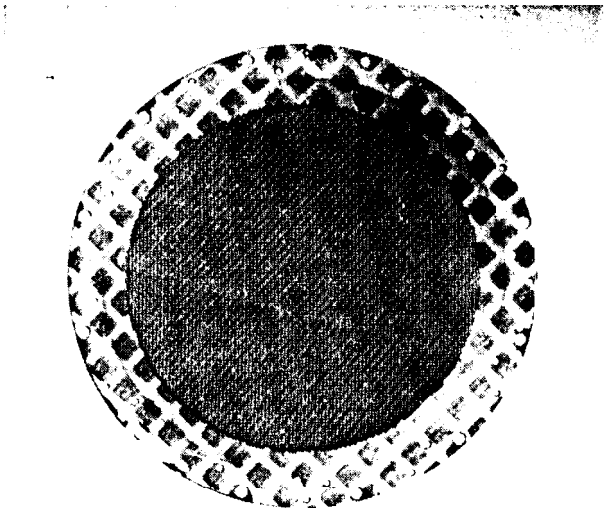

Fig. 3: Decelerator Grid

accclc.rater grid. The bolt circles for the. grid mounting holes arc identical to the. ones on the accelerator grid but clocked 1 SO. The decelerator grids includes clearing holes for screen grid and accelerator grid mounting screw heads. Decelerator hole diameters arc 1.77 mm on average, resulting in an open area fraction for the decelerator grid of 58 %.

Mount Ring Fabrication

In order to save weight for the total assembly and match CTE's with the grids, a carbon-carbon mount ring was fabricated for the. 30-cm grid set, A phonograph of the mount ring is shown in Fig.4. The mount ring was laid up from segments of plain weave fabric made from PAN based Amoco T-300 fiber and phenolic resin (Borden SC1008). Segments of the plain weave fabric arc still visible in the finished product, shown in a closer view in Fig.5. In this figure, the. mount ring is shown before machining of the mounting holes. The lay-up and curing were performed with the help of an aluminum fixture shown in Figs. 6 and 7. The mount ring was laid up in the lJ-shaped crevice formed by the fixture, giving, the ring its shape. After completion of the lay-up, a long slab of silicon rubber was inserted into the crevice, covering the composite lay-up and fixated with a large hose clamp. The entire assembly was then placed in a circulated air oven at 175 ^{o}C for 16 hours for curing. Pressure was provided by thermal expansion of the silicon mandrel.

Table 2: Description of 30-cm Carbon-Carbon Grids

Description of 30-cm Carbon-Carbon Grids	
Common to all Grids	
Grid Material	Carbon-Carbon
Grid Shape	Dished
Beam Diameter (cm)	28.6
Hole Quantity	-15,500
Hole Spacing (mm)	2.21
Screen Grid	
OD (cm)	35.(K)
OD Dish (cm)	33.17
Thickness (mm)	0.46
Hole Dia. (mm)	1.89 (+0.025/-0.009)
Open Area Fraction	66 %
Weight (gram)	43.6
Manufacturing Technique	Laser Drilling
Accelerator Grid	
OD (cm)	38.06
OD Dish (cm)	33.17
Thickness (mm)	0.46
Hole Dia. (mm)	1.126 (+/- 0.02)
Open Area Fraction	23.5 %
Weight (gram)	*80.2*
Manufacturing Technique	Laser Drilling
Decelerator Grid	
OD (cm)	38.06
OD Dish (cm)	33.17
Thickness (mm)	0.46
Hole Dia. (mm)	1.77(+0.008/-0.01)
Open Area Fraction	58 %
Weight (gram)	58.4/60.6"
Manufacturing Technique	laser Drilling
Mount Ring	
ID (cm)	33.17
OD Upper Flange (cm)	35.06
OD Lower Flange (cm)	38.06
Material	Carbon-Carbon
Weight	222.6
Manufacturing Technique	Mechanical

" Two grids weighed

Final machining of the mount ring was performed by Electro-Tech Machining. The mount ring has an 11) of 33.17 cm, equal to the diameter of the. dished area of the grids and two flanges. The screen grid is mounted to the upper flange, shown in Fig. 4. Ceramic spacers arc mounted to the lower flange, which in turo support the accelerator and decelerator grids. The. OD of the upper flange is identical to the OD of the screen grid (i.e. 35.06 cm) and the OD of the lower flange is identical to the ODs of the accelerator and decelerator grids (i.e. 38.06 cm). The lower flange. also features six mounting holes for attaching the mount ring to the ion engine. These mounting holes arc placed uniformly spaced on a 36.19 cm dia. bolt circle. Overall height of the. mount

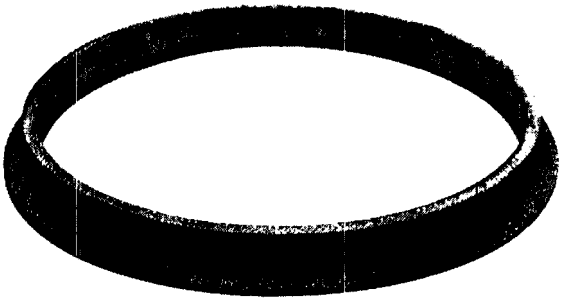

Fig. 4: Carbon-carbon Mount Ring

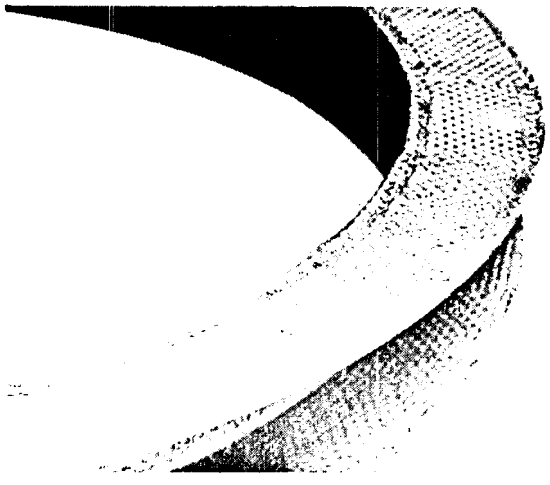

Fig. 5: Close-up of Carbon-Carbon Mount Ring showing Details of Lay-up

Fig. 6: Aluminum Fixture used in Mount Ring Fabrication (Assembled)

Fig. 7: Aluminum Fixture for the Mount Ring (Disassembled)

ring, measured from the bottom surface of the lower flange to the top surface of the upper flange, is 3.48 cm (+0.1/-0.3 cm).

Inspection of the mount ring after the carbonization, graphitiz.alien and CVI phases of the fabrication process revealed that the two flanges (upper and lower) of the ring were not parallel, probably as a result of the high temperature fabrication processes and the fact that the. mount ring was high-temperature treated free-standing, because the alum inum and silicon rubber tooling was not able to withstand the temperatures. The upper flange drops with respect to the lower flange by about 0.2 - 0.6 mm toward the outer edge. of the upper flange depending on location along the circumference.

Figure 8 shows an assembled grid set consisting of the mount ring and two grids, a screen and accck.rater grid. The over-11 grid set mass is 5S0 grams. Although difficult to recognize in Fig. 8, the grids arc mounted dished inwardly, The reason for mounting the grids in this fashion was to minimize the performance impact of the difference in screen and accelerator grid dish depth.s. The screen grid has a slightly larger radius of curvature than the accelerator grid. Mounting the grids dished outward from the engine would have resulted in a larger grid gap between the screen and accelerator grids near the center of the grids and a smaller gap towards the edges. The twain current density distribution of an ion engine generally peaks on the. centerline. By dishing the grid set inward, a smaller grid gap could be maintained near the center of the grid, leading to a higher extractable beam current.

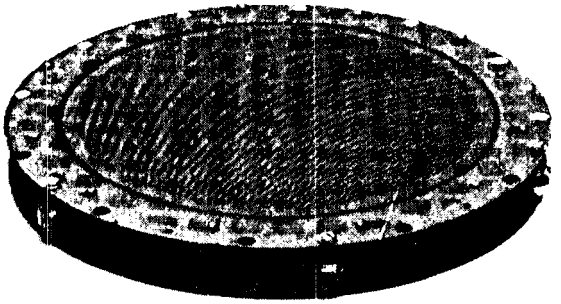

Fig. 8: Assembled Two-Grid 30-cm dia. Carbon-Carbon Grid SC(

Grid-Set Inspection

Following the fabrication of the grids, measurements of grid hole. diameters, the. radius of curvature, and the grid gap between the screen and accelerator grid of the mounted on the carbon-carbon mount ring were performed.

Measurement of Grid Hole Diameters

The measured grid hole sizes for the different grids are given in Table.2. Grid hole measurements were performed with a MicroXcel optical measurement system equipped with a Ram Optical Instrumentation camera. Measurements using this system arc conducted by focusing a camera with a fixed focal length on onc ho]c edge.. A highly magnified image (up to 250x magnification) is transmitted for display on a monitor which allows the operator to adjust the focus of the, image by moving the camera platform accordingly . The position of the camera platform in x-, y-, and z-coordinates is determined. The camera is then moved until the opposite hole side is brought into focus and the system provides an x, y-, and z-read out for this ncw position. Noting the. distance the camera has traveled in x-, y-, and z-directions allows the determination of the hole diameter.

Inspection of Grid Curvature

Measurements of the radius of curvature of the grids were performed with the same optical technique used to determine the grid hole diameter described above. Here, the grid was placed onto a flat bench (equal or less than 0.008 mm/m variation), serving as the horizontal reference plane, with the convex side of the grid facing up. The fixed fecal-length camera was first focused onto the top (convex) surface of the grid by positioning it properly with respect to the grid surface. Then, by moving it downward in the +z direction (compare with Fig. 9), the camera was focused onto the flat bench surface beneath the grid. Noting the shift in the z-coordinate of the camera platform allowed the determination of the height of the top surface above the surface of the fiat bench. The x- and y-coordinate.s were also noted to deter-mine a height profile of the grid. An (x ,y,z) coordinate system was defined with respect to the grid as shown in Fig. 9. The origin was placed at the. center (apex) of the. grid and the + x direction pointed toward the clocking hole identified try the arrow-mark in Figs. 4 through S. The +z -axis faced downward toward the bench.

The measured height of the. upper grid surface above the bench surface (labeled z in Tables 3 through 5 below') was then compared with the calculated value for this height (labeled z_{calc} in the tables below) based on the design value for the radius of curvature. For a spherical dish, this value is given by

$$z_{calc} = h' \sin\left(\cos^{-1}\frac{\sqrt{x^2 + y^2}}{R}\right) \cdot \sqrt{R^2 - s^2} \qquad (2)$$

} lere R is tbc radius of curvature for the top surface of the. grid, x and y arc the coordinates of the grid location under consideration, with the origin located at the grid, and s is the radius of the dished area as shown in Fig. 10. Note that the design value for the radius of curvature was given for the lower grid surface, while the height z of the grid surface is measured to the top surface of the grid,

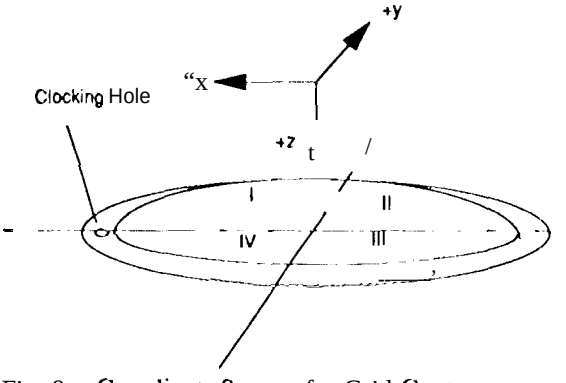

Fig. 9: Coordinate System for Grid Contour Measurements

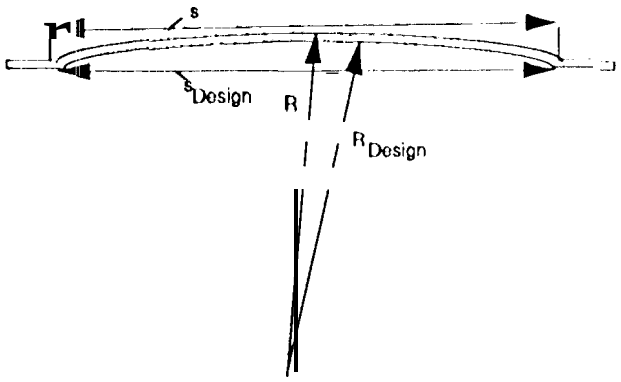

Fig. 1(): Geometry of the Dished Grid

For this reason, the value for R in Eqn (1) has to be increased try the grid thickness, i.e.

$$R = R_{Design} - t \qquad (3)$$

where R_{Design} is the specified design value for the radius of curvature as measured at the lower grid surface, i.e. 2,032 mm and t is the grid thickness of 0.46 mm. Note further that duc to measuring the grid height to the upper grid surface, ideall y the. value. for the radius of the. dish, s, also has to be increased according to

$$s = s_{Design} \left(1 + \frac{t}{R_{Design}}\right) \qquad (4)$$

where s_{Design} is the specified design value for s, i.e.. 16S,9 mm and t is the grid thickness again. The value in brackets is very close to unity and subsequently the value for s was approximated by the design values s_{Design} given for the lower surface.

Using the calculated value for the upper grid surface height over the horizontal reference plane (i .e. the bench), z_{calc}, the difference of the measured height from the design height can be determined and the deviation from the ideal grid shape can be quantified. q'able 3 lists the corresponding values for onc of the two screen grids that were fabricated. From Table 3, it is clearly evident that the screen grid surface is significantly less curved than the design intended. The differences between actual height and the design value. of the height vary across the grid, decreasing toward the edges of the grid. However, close to the center of the grid, the apex of the grid surface is about 1 mm lower than its design value. Even though the grid does not appear to be perfectl y spherical, an approximate radius of curvature of the screen grid bawd on the. curvat urc measurements may be determined from

$$R_{actual} = \frac{z_{max}^2 + s^2}{2\, z_{max}} - d \qquad (5)$$

where d is the grid thickness (0.46 mm). For a maximum height of about 5.7 mm, the approximate radius of curvature is 23.7 cm, or about 3.5 cm larger than its design value. of 20.3 cm.

Inspecting q'able 4, the accelerator grid also shows a flattened profile. when compared with its design contour, however, the differences arc less pronounced than for the screen grid. Here, the actual grid apex height falls short by about 0.3 mm from its design value. Also, slight non-symmetries in the profile of the accelerator grid can be noted when inspecting grid heights measured along the horizontal and the diagonal intersecting the second and fourth quadrant of the grid (compare with Fig. 9). These non-symmetries may be duc to grid warping and at opposite sides of the grids at equal distance from the. apex these differences amount to about 0.3 - 0.4 mm. Even though a balanced [0°/+60°/-60°] lay-up was chosen to limit grid warpage, slight imbalances in the. lay-up may have occurred duc to small, localized differences in the thickness of the. prepreg material caused by splits in the tape for example.

Based on the. measured apex height of approximately 6.45 mm, the radius of curvature may be estimated using Eqn. (5) with the assumption that the grid profile is spherical. The. radius of curvature of the accelerator grid is then determined to 21.35 cm, almost 2. cm smaller than the value calculated for the. screen grid. This difference in radius of curvature for the two grids is the source of the difficulties encountered when trying to mount thcm with an outward dish, The shallower screen grid mounted beneath the more sharpl y curved accelerator grid will leave a bigger gap between the two grids near the center (see Fig. 11). By mounting the grids with the convex side of the dish facing toward the engine, the. sharper curved accelerator grid mounted above. the screen grid leaves a smaller grid gap near the grid center. It should be noted that changing the grid orientation in this fashion was only possible because placement of the. grid holes was not compensated for the grid curvature and holes were cut parallel to the axis of rotational symmetry for the grid rather than normal to the grid surface.

l'able 3: Contour Measurements of Screen Grid

x (mm)	y (mm)	z (mm)	z calc (mm)	z-z calc (mm)	delta z (%)
Vertical					
125.94	-2.02	2.64	2.87	-0.23	-8.01
98.71	-2.29	3.81	4.38	-0.s7	-12.92
73.06	-3.41	4.70	5.46	-().76	-13.96
31.42	-4.93	5.63	6.53	-0.90	-13.79
6.29	-9.39	5.75	6.75	-1.00	-14.80
5.69	2.25	5.78	6.77	-0.99	-14.56
5.32	-0.09	5.79	6.77	-0.98	-14.55
4.06	6.57	5,72	6.76	-1.05	-]5.50
-24.14	5.54	5.69	6.63	-0.94	-14.18
-48.90	4.63	5.16	6.]8	-1.02	-16.50
-105.08	2.57	3.37	4.06	-(),69	-17.06
Horizontal					
9.56	-127.46	2.53	2.75	-0.22	-7.97
9.09	-96.67	3.85	4.46	-0.61	-13.67
8.84	-6s.80	4,88	5.69	-0.81	-14.25
8.42	-44.45	5,46	6.27	-0.82	-13.00
7.07	-19.55	5.77	6.67	-0.90	-13.54
S.69	17.77	5.68	6.69	-1.01	-15.06
4.91	39.]3	5.32	6.40	-1.08	-16.83
3.80	63.55	4.74	5.78	-1.04	-18.05
2.84	89.60	3.96	4.80	-0.84	-17.55
1.63	122.63	2.81	3.07	-0.26	-8.54
Diagonal 1-Ill					
97.87	91.99	2,26	2.33	-0.07	-3.18
66.24	62.15	3,93	4.7s	-0.81	-17.13
39.39	37.81	5,02	6,04	-1.02	-16.88
20.35	23.09	5.51	6.s4	-1. (M	-15.82
-9.11	-16.05	5.78	6.69	-().92	-13.72
-2.8.91	-29.84	5.50	6.35	-0.86	-13.48
-51.01	-52.07	4.66	5.47	-0,81	-14.89
-73.55	-65.10	3.76	4.40	-0.64	-14.63
-91.86	-82.15	2.72	3.04	-0.32	-10.47
-100.10	-96.39	1.99	2.02	-0.04	-1.7s
Diagonal II-IV					
-90.07	88.38	2.69	2.86	-0.16	-5.67
-62.63	58.89	4.25	4.96	-0.71	-14.31
-43.53	37.20	5.12	5.97	-0.85	-14.25

Table 4: Contour Measurements of Accelerator Grid

x (mm)	y (mm)	z (mm)	z calc (mm)	z-z calc (mm)	Delta z (%)
Vertical					
137.21	2.02	2.09	2.14	-0.05	-2.45
112.00	0.73	3.60	3.69	-0.09	-2.52
84.24	1.41	4.84	5.03	-0.19	-3.88
48.43	1.21	5.94	6.20	-0.26	-4.14
21.15	0.87	6.41	6.67	-0.26	-3.89
12.13	0.44	6.40	6.74	-0.34	-5.02
0.10	1.70	6.45	6.78	-0.32	-4.77
-4.68	2.19	6.48	6.77	-0.29	-4.35
-24.34	2.39	6.26	6.63	-0.37	-5.54
-44.17	1.74	6.01	6.30	-0.29	-4.61
-59.47	2.10	5.66	5.91	-0.24	-4.11
-82.91	3.01	4.84	5.08	-0.2s	-4.83
-102.52	4.58	4.04	4.19	-0.14	-3.39
-137.24	1.07	2.07	2.14	-0.07	-3.44
tlorizontal					
0.85	-131.01	2.60	2.55	0.0s	1.86
1.01	-69.39	5.38	5.59	-0.22	-3.86
2.37	-55.15	5.79	6.03	-0.24	-3.97
3.11	-38.22	6.15	6.42	-().27	-4.20
1.13	-14.89	6.44	6.72	-().28	-4.1s
1.98	-6.63	6.44	6.77	-0.32	-4.76
1.13	3.18	6.45	6.78	-0.32	-4.74
0.34	10.48	6.44	6.75	-0.31	-4.62
0.15	16.78	6.38	6.71	-0.33	-4.89
1.58	35.25	6.18	6,47	-0.29	-4.51
1.19	58.13	5.64	5.95	-0.31	-5.17
1.04	79.65	4.91	5.22	-0.30	-5.83
0.33	100.93	3.98	4.27	-0.29	-6.73
1.20	118.51	3.05	3.32	-0.27	-8.10
1.31	133.14	2.18	2.41	-0.23	-9.43
Diagonal 1-111					
83.37	76.6S	3.39	3.62	-0.23	-6.41
71.22	63.62	4.28	4.53	-0.26	-5.64
57.47	52.01	5.03	5.30	-0.27	-5.05
45.50	38.67	5.57	5.90	-0.33	.5.55
31.6]	25.73	6.05	6.37	-0.32	-4.97
?6.70	20.76	6.18	6.50	-0.31	-4.80
18.01	12.67	6.32	6.66	-0.34	.5.09
11.83	6.76	6.38	6.73	-0.35	-5.26
4.00	-1.12	6,47	6.77	-0.30	-4.49
-7.26	-12.42	6,44	6,73	-0.29	-4.25
-19.78	-21.83	6.31	6.56	-0.25	-3.85
-28.08	-34.07	6.05	6.30	-0.25	-3.98
-47.48	-46.87	5.44	5.68	-0.24	-4.31
-54.30	-58.3S	4.99	5.21	.0.22	-4.23
-66.37	-67.93	4.43	4.56	-0.13	-2.86
-79.90	-79.57	3.60	3.65	-0.05	-1.40
-88.68	-90.19	2.79	2.84	-0.05	-1.74
-97.87	-98.88	1.99	2.01	-0.02	-0.82
Diagonal II-IV					
-95.16	93.60	2.23	2.39	-0.16	-6.81
-86.30	85.65	2.92	3.14	-0.22	-7.08
-75.29	74.08	3.79	4.03	-0.24	-6.07
-61.78	62.73	4.55	4.87	-0.32	-6.59
-48.98	47.28	5.36	5.64	-0.28	-4.93
-37.64	36.78	5.77	6.10	-0.33	-5.43
-19.58	24.10	6.18	6.54	-0.36	-5.48
-10.82	13.82	6.33	6,70	-0.38	-5.60
2.74	-1.06	6.50	6.78	-0.27	-4.04
11.24	-10.35	6.39	6.72	-0.33	-4.87
24.49	-25.7S	6.20	6.47	-0.26	-4.09
36.52	-37.95	5.86	6.10	-0.23	-3.83
50.64	-51.96	5.32	5.48	-0.16	-2.98
61.88	-62.65	4.71	4.87	-0.16	-3.35
75.31	-74.22	3.89	4.03	-0.13	-3.33
94.92	-89.46	2.54			1.86

Table 5: Contour Measurements of Decelerator Grid

x (mm)	y (mm)	z (mm)	z calc (mm)	z-z talc (mm)	Delta z (%)
Horizontal					
136.09	4.50	1.81	2.21	-0.40	-18.00
74.51	0.24	4.74	5.41	-0.67	-12.32
53.99	0.64	5.44	6.06	-0,63	-10.31
42.37	-0.04	5.71	6.34	-0.62	-9.84
19.19	-0.90	6.09	6.69	-0.60	-8.92
4.72	0.10	6.18	6.77	-0.60	-8.79
3.39	-0.21	6.19	6.78	-0.59	-8.64
-4.45	-0.05	6.20	6.77	-0.58	-8.53
-29.15	1.06	5.97	6.57	-0.60	-9.13
-44.45	0.73	5.74	6.29	-0.56	-8.84
-65.37	0.50	5.19	5.73	-0.53	-9.29
-94.69	0.82	4.07	4.s7	-0.50	-11.04
-117.77	0.39	2.99	3.36	-0.38	-11.17
-135.61	1.26	1.96	2.25	-0.29	-12.90
Vertical					
1.60	-134.72	2.09	2.31	-0.22	-9.41
0.30	-106.55	3.48	3.98	-0.50	-12.51
-0.85	-80.61	4.64	5.18	-0.54	-10.39
-0.94	-58.77	5.37	5.93	-0.56	-9.46
-0.58	-40.28	5.75	6.38	-0.63	-9.93
-0.48	-23.09	6.06	6.65	-0.59	-8.82
0.75	-0.94	6.17	6.78	-0.60	-8.90
0.73	7.37	6.21	6.76	-0.56	-8.27
1.18	30.16	5.95	6.55	-0.60	-9.19
1.87	49.91	S.60	6.16	.0.56	-9.14
2.76	82.88	4.48	5.09	-0.61	-11.95
3.28	109.30	3.30	3.83	-0.53	-13.94
6.35	134.66	1.95	2.30	-0.36	-15.49
Diagonal I-III					
89.61	99.71	2.05	2.35	-0.30	-12.94
69.74	77.11	3.55	4.12	-0.57	-13.87
45.83	55.89	4.91	5,49	-0.58	-10.52
26.68	39. *O	5.64	*6.2?*	-0. s9	-9.4s
9.42	22.07	6.07	*6.64*	-0.56	-8.49
-10.74	-6.31	6.18	*6.74*	-0.56	-8.31
-29.04	-22.78	5.88	*6.44*	-0.s7	-8.81
-50.16	-37.39	5.28	5.81	-0.54	-9.27
-62.61	-50.16	4.62	*5.J9*	-0. s7	-11.05
-75.35	-63.71	3.86	*4.38*	-0.52	-11.82
-88.75	-80.25	2.87	*3.25*	-0.39	-11.84
-96.84	-92.78	2.10	*2.35*	-0.25	-10.45
Diagonal II-IV					
-105.98	82.66	2.06	2.33	-0.27	-11.68
-94.27	75.26	2.84	3.20	-0.36	-11.12
-79.66	57.90	3.89	4.39	-0.50	-] 1.38
-59.40	47.13	4.84	5.36	-0.52	-9.73
-39.46	31.61	5.50	6.15	-0.65	-10.61
-25.50	19.44	5.89	6.53	-0.64	-9.77
-10.60	7.39	6.14	6.74	-0.59	-8.80
21.87	-25.03	5.96	6.51	-0.54	-8.34
33.24	-30.05	5.6S	6.28	-0.64	-10.15
54.04	-63.23	4.48	5,08	-0,59	-11.72
7211	-67.67	3.79	4.37	-0.58	-13.24
103.44	-87.99	1.91	2.24	0.33	14.69

The data in Table 5 indicate that the decelerator grid contour has flattened to a degree ranging between the radii of curvature of the screen and accelerator grid. The apex of the grid is about 6.2 mm, or about 0.6 mm lower than its design value. The equivalent radius of curvature according to Eqn. (5) is 22.21 cm. Again, some non-symmetries can be noted in the decelerator grid height distribution, in particular along the horizontal axis listed in Table 5. However, differences at opposite sides of the grid along this horizontal axis differs by only 0.1 mm and may again be duc to a slight warpage of the. grid.

The height difference between the actual grid height and its design value at the center of the. grid correlates well with the open area fraction of the grid (Fig. 1'2). The larger the open area fraction of the grid, the. larger is the shortfall in grid height at the center from its design value. Although not yet fully understood, it is possible that residual stresses that remained in the grid panel after fabrication may be responsible for this behavior. Since for the grids with the larger open area fraction less grid material remains to counter these residual stresses, they shallow to a higher degree than the grids with lower open area fractions.

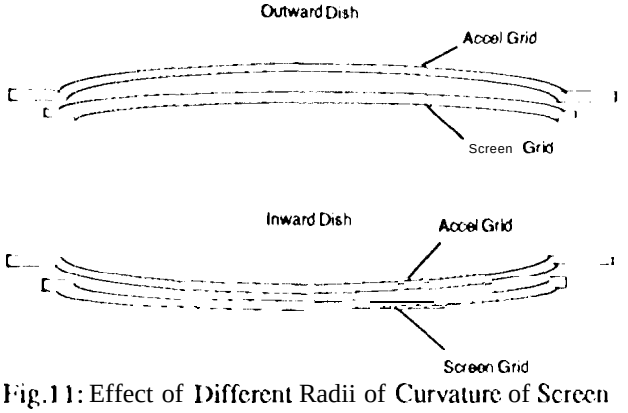

Fig.11: Effect of Different Radii of Curvature of Screen and Accelerator grid on Grid Mounting

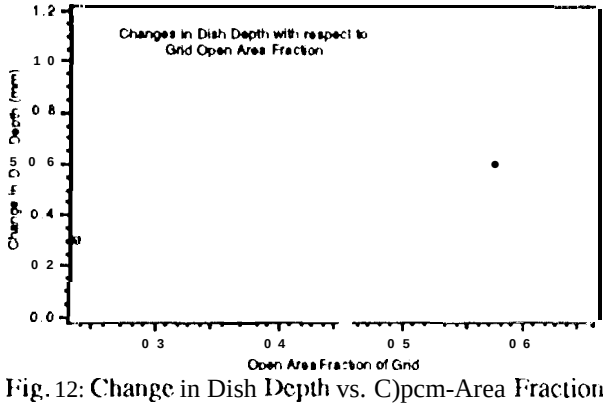

Fig. 12: Change in Dish Depth vs. C)pcm-Area Fraction

Inspection of Grid Gaps

Grid gap measurements were performed on the assembled grid set consisting of the inward di.shed screen and accelerator grids, The same optical measurement technique used in the grid hole determination and grid contour measurements was used, Here, the grid set was placed on the flat bench described above with the. screen grid facing upward and the camera was first focused onto the screen grid top surface near the edge of a grid hole. Next, by moving the fixed-focal length camera downward, it was foc used onto the. accelerator grid surface beneath the screen grid and the. shift in z-coordinate was determined. Duc to the S} IAG optics design of the accelerator grid a sufficient amount of grid surface was visible through the screen gi id aperture. After subtracting the screen grid thickness from the observed shift in the ?.-coordinatc the grid gap was obtained.

Table 6 lists grid gap measurements for the assembled grid set shown in Fig. 11. The x- and y-coordinates arc measured again from the center of the screen grid. As can be seen, close to the grid center grid gap values of about 0.5 mm arc obtained which is close to typical grid separation values. Near the. edges the grid gap increases as would be expected from the. difference in radius of curvature for the. screen and accelerator grid. The larger grid gaps near the grid edges arc obviously undesirable, however, since extracted beam current densities arc lower near the edges of the beam extraction area, grid performance may be compromised less than would be the case if the larger grid gaps occurred near the grid center, depending on the ion beam current density profile.

Grid Testing

Test Set-up

The grid set shown in Fig. 8 was mounted to a J-series type thruster[13,14] that has been modified for inert gas operation as described in Ref. 15. Figure 13 shows the operating J-.scrics thruster with the inward dished carbon-carbon grid set attached. 'f 'ests were performed in a 2.4-m diameter and 5.5-m long stainless steel vacuum chamber equipped with three oil diffusion pumps. The pumping speed on xenon is approximately 14,000 1/s. Vacuum chamber pressure measurements were made with an ion gauge directly calibrated on xenon. Typical vacuum pressures during engine operation were 2.5-4 x 10"^{3} Pa (2 -3 x 10^{-5} q'err). The no-load pressure in the facility is less than 4 x 1 0^{-5} Pa (3 x 10'7 Torr).

3'able 6: Grid Gap Measurements

X (mm)	y (mm)	z (mm)
Vertical		
139.47	-2.54	1.11
128.09	-2.01	0.82
116.28	-2.44	0.64
100.18	-0.25	0.43
78.21	2.54	0.27
48.95	0.30	0.33
35.03	0.76	0.51
27.33	-0,10	0.44
14.94	-0.56	0.60
6.10	0.64	0.58
-1.73	-0.28	0.49
-3.91	0.05	0.55
-6.68	2.36	0.60
-16.43	-0.43	().62
-30.38	-0. ?8	0.69
-45.31	-0.43	0.64
-s9.79	-0.36	0.67
-76.43	-0.23	().72
-96.60	-3.6(,	().72
-118.52	-4.50	0.92
Horizontal		
-1.04	-140.00	1.03
0.5]	-98.88	0.51
1.85	-112.75	0.63
-2.01	-73.41	0.45
-1.24	-50.42	0.45
-2.26	-38.58	0.52
-2.90	-21.34	0.57
-4.04	9.70	0.61
-0.91	31.01	0,61
0.28	57.99	0.57
-1.60	77.55	0.61
-2.18	99.()()	0.61
-1.83	118.26	0.80
-3.58	141.55	0.98
Diagonal I-III		
93.22	104.06	0.80
71.09	72.52	0.52
39.95	37.62	0.43
-30.56	-19.43	0.63
-64.97	-46.02	0.73
-109.42	87.73	1.07
Diagonal IV-II		
79.78	-112,17	0.98
38.13	-48.74	0.33
18.67	-27.74	0.42
-18.03	16.08	0.64
-45.19	56.21	0.66
-68.86	89.66	0.85
-80.44	112.47	1.20

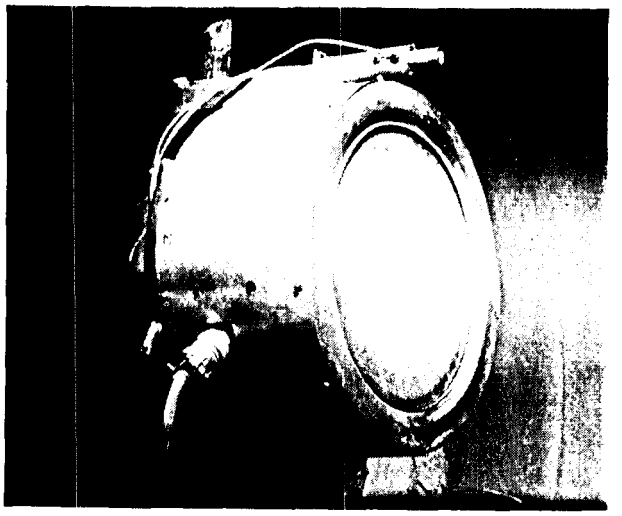

Fig. 13: 30-cm-dia. Carbon-Carbon Grid Set mounted on J-Series Type Thruster. Two-Grid System, Dished Inward.

The propellant flow control system was described in detail in **Ref. 12. This flow system was designed for the.** segmented ion thruster (SIT) described in that reference and consisted of four parallel branches for the four segments of the. SIT engine. Here, only onc of the. four branches was used. The same set of power supplies as used in the SIT thruster tests was used, consisting of laboratory power supplies throughout[12] For the main discharge 0-50 V and O-20 A supplies from Power Ten, inc. arc used. The high voltage supply is a custom 12 kW (6 A and 2 kV) supply made by Spellman. The cathode and neutralizer start supplies arc made by Kepco.

Test Procedures

Perveance Measurements

The perveance of an ion engine grid describes its ability to extract current from the discharge chamber. Perveance measurements were performed by keeping the screen current (beam current plus accelerator impingement current) constant while. varying the total grid voltage between the. screen and accelerator grids and measuring the accelerator impingement current. In order to ensure a constant screen current, the discharge current was adjusted accordingly. The screen current is slightly larger than the beam current by an amount equal LO the accelerator impingement current.

Electron Backstreaming Measurements

Electron backstreaming occurs when the. (negative.) accelerator grid voltage becomes too small (in magnitude) to shield the discharge chamber plasma from electrons in the beam plasma, Backstreaming electrons cause an increase in screen grid current, indicating that the electron backstreaming limit has been reached. Here, accelerator voltage was lowered manually to the point of electron backstreaming onset.

Results

Perveance Measurements

Figure 14 shows the perveance data obtained with the inward dished 30-cm carbon-carbon grid set at screen currents of 1.7 A and 1.0 A. In both cases screen current varied slightly during the course of taking the data shown in Fig.4. Perveance limits for the. 1.0 A screen current are around 1 kV and for the 1.7 A case around 1.4 kV. These values are compared in Fig.14 with values obtained previously[7,b] for a molybdenum grid set mounted to the. same thruster, The molybdenum grid set consisted of a screen and accelerator grid with same hole geometries as the grids used in the. carbon-carbon set. However, the molybdenum set was dished outward and a smaller grid gap of 0.66 mm throughout the system. As a result, perveance limits were lower for the molybdenum set. At 1.76 A and 1.01 A beam currents the perveance limits were 1.15 kV and about 980 V. Due to the shallow knee in the. 1.01 A curve for the molybdenum set it is difficult to determine the. perveance limit precisely. The higher accelerator grid currents for the carbon-carbon grid set arc a facility effect. The carbon-carbon test was performed at a background pressure of 2-4 x 10^{-3} Pa (2-3 x 10^{-5} Torr) while the molybdenum test was conducted in a different, cryo-pumped facility at a back pressure of merely 5 x 1 0^{4} Pa (4 x 10^{-6} q'err), resulting in lower charge exhange ion production.

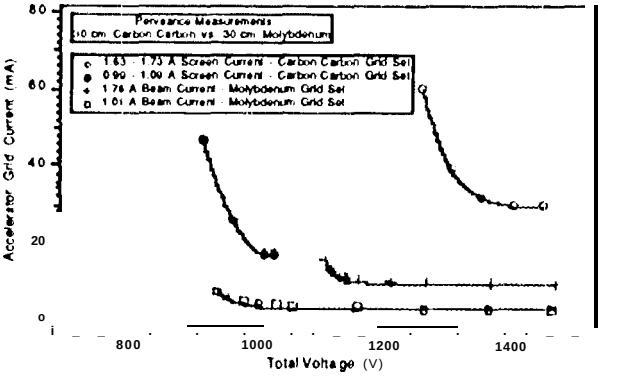

Fig.14: Perveance Measurements for 30-cm dia. Dished Carbon-Carbon and Molybdenum Grids

Electron Backstreaming Measurements

Electron backstreaming data arc shown in Fig. 1S. The minimum accelerator voltage at a screen current of about 1 A is -90 V. The beam voltage was 950 V in this case, translating into a maximum net-t~total voltage ratio of 0.91. For 1.7 A screen current, the minimum accelerator voltage was found to be around -130 V. } lere the beam voltage was 12S0 V, corresponding to a maximum net-to-total voltage ratio of 0.906, i.e. slightly less than for the 1 A value. The corresponding value.s for the closer gapped molybdenum set mentioned above were -144 V arid-121 Vat beam currents of 1.76 A and 1.01 A, respectively.

Conclusions

Two 30-cm carbon-carbon grid sets were fabricated, including two light-weight carbon-carbon mount rings, in order to study the feasibility of fabrication, assembly and operation of large. diameter carbon-carbon grid. Screen, accelerator and decelerator grid optics were manufactured in order to also test the. carbon-carbon grids in SAND optics configuration, The grids were designed to be retrofittable to the current 30-cm NSTAR engine design.

The carbon-carbon panels were fabricated from unidirectional tape using a [0°/+60°/-60°]$_s$ lay-up resulting in the strongest quasi-isotropic carbon-carbon known to the authors. High fiber volume fractions of 57% led to a flexural modulus for these. panels of up to 27S MPa or about 80% of the corresponding value for molybdenum. High flexural moduli arc a crucial material property for ion engine grid materials since stronger grids will flex to a lesser degree duc to electrostatic stresses or launch vibrations.

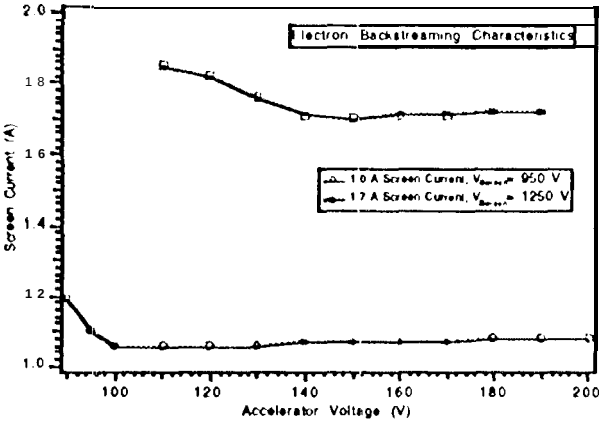

Fig. 15: Electron Backstreaming at Screen Currents of 1.7 A and 1.0A.

A laser-machining process was used to machine grid hole apertures. Grid contour measurements performed after fabrication revealed that radii of curvature obtained for the grids were larger than specified, with larger radii of curvature correlated with higher grid open area fractions. Screen, accelerator and decelerator radii of curvature were 23.7 cm, 21.4 cm and 22.2 cm, respectively, compared to the specified design value of 20.3 cm. Actual radii of curvature were estimated bawd on height measurements at the grid center, assuming a spherical grid contour. However, small differences in grid height at opposite locations of the grid were noted and arc on the. order of 0.1 mm for the accelerator grid and 0.3 - 0.4 mm for the decelerator grid could be noted, indicative of a slight warping of the grids.

The large difference in radii of curvature between the. screen and accelerator grid dictated that the grids be mounted dished inwards in order to obtain the desired grid-to-grid separation on the centerline. Perveance and electron backstreaming were performed with this grid set. The perveance limit at a 1 A screen current is approximately 1 kV and for a 1.7 A screen current it was around 1.4 kV.

Acknowledgements

The authors would like to thank Mr. Alison Owens, Mr. William Thogmartin, and Mr. Robert Toomath for assembling the grid sets and support hardware. Wc would like to especially thank Mr. Phil Gossmann for performing the extensive grid hole, grid contour and grid gap measurements. The authors thank Mr. Vince Rawlin for lending his expertise to this activity and Mr. Frank Curran and NASA Lewis Rc.search Center for sponsoring this work.

References

1. Mueller, J., Brophy, JR., and Brown, D.K., "Endurance Testing and Fabrication of Advanced 15-cm and 30-cm Carbon-Carbon Composite Grids", AIAA Paper 95-2660, 3 1st Joint Propulsion Conference, San Diego, CA, July 10-12, 1995.

2. Brophy, J. R., Mueller, J., and Brown, 1). K., "Carbon-Carbon Ion Engine Grids with Non-Circular Hole Apertures", AIAA Paper 95-2662, 31s[Joint

Propulsion Conference, San Diego, CA, July 10-12, 1995.

3. Mueller, J., Brophy, J. R., Brown, D. K., and Gamer, C.E., "Performance Characterization of 1 S-cm Carbon-Carbon Composite Grids", AIAA Paper 94-3118, 3oth Joint Propulsion con ference, Indianapolis, IN, June 27-29, 1994.

4. Mueller, J., Brown, D. K., Gamer, C.E., and Brophy, J.R., "Fabrication of Carbon-Carbon Grids for Ion Optics", IEPC Paper 93-112., 23rd International Electric Propulsion Conference, Sep. 13-16, 1993, Seattle, WA.

5. Gamer, C.E. and Brophy, J.R., "Fabrication and Testing of Carbon-Carbon Grids for Ion Optics", AlAA Paper 92-3149, 28th Joint Propulsion Conference, Nashville, TN, July 6-8, 1992.

6. Meserole, J.S. and Rorabach, M.E., "Fabrication and Testing of 1 S-cm Carbon-Carbon Grids with S I it Apertures", AlAA Paper 95-26.51, 31s1 Joint Propulsion Conference, San Diego, CA, July 10-12, 1995.

7. Meserole, J.S. and Hedges, D.E., "Comparison of Erosion Rates of Carbon-Carbon and Molybdenum Ion Optics", IEPC Paper 93-111, 23rd International Electric Propulsion Conference, Seattle, WA, Sept. 13-16, 1993.

8. Hedges, D.E. and Meserole, J. S., "Demonstration and Evaluation of Carbon-Carbon Ion Optics", *Journal of f'repulsion and Power*, **Vol. 10, No.** 2, March-April 1994, pp.255-261.

9. Meserole, J. S., "Measurement of Relative Erosion Rates of Carbon-Carbon and Molybdenum Ion optics", AIAA Paper 94-3119, 30th Joint Propulsion Conference, June 27-29, 1994, Indianapolis, IN.

10. Brown, D.K. and Gamer, C.E., "Carbon/Carbon for Ion Optics", JANNAF Joint Propulsion Meeting, November 1993.

11. Blandino, J.J., Goodwin, D. G., Gamer, C.E. and Brophy, J.R., "Evaluation and Development of Diamond Grids for Ion Optics", AIAA Paper 95-2663, 31st Joint Propulsion Conference, San Diego, CA, July 10-12, 1995.

12. Brophy, J.R., Mueller, J., Pless, L.C., Goodfellow, K. M., and Anderson, J.R., "Segmented Ion Engine Operation and Performance", AlAA Paper 94-2851, 30th Joint Propulsion Conference, June 27-29, 1994, Indianapolis, IN.

13. Bechtel, R. T., "The 30 cm J Series Mercury Bombardement Thruster", AIAA Paper 81-0714, 15th International Electric Propulsion Conference, Las Vegas, NV, April 21-23, 1981.

14. Rawlin, V. K., "Operation of the J-Series Thruster Using Inert Gas", AIAA Paper 82-1929, 16th International Electric Propulsion Conference, Ncw Orleans. 1.A, Nov. 17-19, 1982.

15. Brophy, J. R., Polk, J.E., and Pless, L. C., "Test-to-Failure of a Two-Grid, 30-cm dia. Ion Accelerator System", IEPC Paper 93-172, 23rd International Electric Propulsion Conference, Seattle, WA, Sept. 13-16, 1993.

16. Polk, J.E., Pers. Comm., JPL, June 28, 1996.